ARTICLE IN PRESS

Corrosion Science xxx (xxxx) xxx–xxx

Contents lists available at ScienceDirect

Corrosion Science

journal homepage: www.elsevier.com/locate/corsci

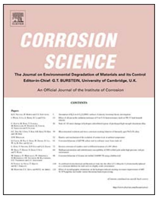

Corrosion of Fe-Ni-Cr alloys with various aluminum additions in a carburizing-oxidizing atmosphere at 900 °C

S. Liu[a,b], J. Shen[b], X.H. Guo[b], L.L. Liu[b,c], Y. Niu[b,*]

[a] College of Materials Science and Energy Engineering, Foshan University, 528000 Foshan, Guangdong, China
[b] University of Chinese Academy of Sciences, Institute of Metal Research, 110016 Shenyang, China
[c] Live Working Center of State Grid Corporation of Hunan, 410000 Changsha, China

ARTICLE INFO

Keywords:
A. Alloy
B. SEM
C. Carburization
C. Oxidation
C. High temperature corrosion

ABSTRACT

The corrosion behavior of Fe-19Ni-13/21Cr-*x*Al ($x = 0, 2, 6$ at.%) alloys in a carburizing-oxidizing atmosphere was compared with that in a purely carburizing atmosphere at 900 °C. The presence of oxygen did not improve the corrosion resistance of the two alloys Fe-19Ni-13Cr-*x*Al ($x = 0, 2$ at.%), while oxygen reduced the carbon attack significantly for the other alloys. The extent of the carbon attack decreased with the increase of the aluminum content, except for the addition of 2 at.% Al to Fe-19Ni-13Cr, which did not reduce the carbon attack. Addition of sufficient aluminum promoted the formation of external Cr_2O_3.

1. Introduction

Carburization and metal dusting are two types of corrosion often occurring on austenitic Fe-Ni-Cr alloys in carburizing atmospheres at high temperature. For alloys exposed to gas mixtures with carbon activity (a_C) less than 1, carburization often occurs with production of internal carbides, producing an embrittlement and reducing the mechanical properties of the alloys [1]. Conversely, metal dusting is catastrophic and frequently occurs in gas mixtures with $a_C \geq 1$: in this case the surface alloy layers are converted into mixtures of carbides, carbon coke and metal particles [2]. Till now, the mechanisms of the above two corrosion modes have been widely studied [1–5].

A possible method to inhibit the carbon attack relies on the formation of continuous and slowly growing Cr_2O_3 scales which are protective in oxidizing environments [6]. However, at high temperatures they do not offer good protection due to evaporation and formation of volatile hydroxide species. Beyond that, chromium may react with carbon and form stable carbides in alloys exposed to gas mixtures with high carbon activities. This will result in the depletion of chromium in a subsurface alloy zone and suppress the formation of external Cr_2O_3 scales. However, small additions of aluminum to Fe-Ni-Cr alloys may lead to the formation of external Al_2O_3 scales, which are more stable than Cr_2O_3 and may offer a much better protection at higher temperatures in many aggressive environments [7]. Till now, the critical concentrations of aluminum needed to form protective scales in gas mixtures containing high carbon activities have been widely studied [8–10]. However, the synergic effect between chromium and aluminum on the prevention of the carbon attack to the alloys has not been examined so far.

The aim of this paper is to investigate the high temperature corrosion of austenitic Fe-Ni alloys with various chromium and aluminum additions in a gas mixture containing two oxidants, carbon and oxygen (denoted as C—O), for a better understanding of their corrosion mechanism. Moreover, the interaction between chromium and aluminum and the effect of their oxides on the general behavior of these alloys will be discussed in this paper.

2. Experimental procedures

Six alloys with nominal composition (all in at.%, if not specified) Fe-19Ni-13/21Cr-*x*Al ($x = 0, 2, 6$) were prepared by vacuum induction melting using mixtures of high purity metals (wt.%) (99.9Fe, 99Cr, 99.9Ni, 99.7Al) and then cast in cylinders of 5 cm diameter, 10 cm high. The alloy ingots were subsequently annealed in 1 atm argon at 1000 °C for 36 h to release the residual stresses and achieve a better equilibration. Their actual composition, measured by ICP spectrometry analysis, is shown in Table 1. The ternary phase diagram of Fe-20Ni-Cr (mass%) system is shown in Fig. 1 [11]. The alloy Fe-19Ni-21Cr-6Al, whose microstructures has already been reported elsewhere [12], is composed of a mixture of a γ-phase matrix plus an even distribution of γ' precipitates richer in chromium. The other alloys are all single γ-phase fcc. Samples with a size of 10 × 8 × 1.5 mm were cut from the ingots using a line saw and a 1 mm hole (required for suspension) was drilled near one edge. All these specimens were mechanically abraded on

---

[*] Corresponding author.
E-mail address: yniu@imr.ac.cn (Y. Niu).

https://doi.org/10.1016/j.corsci.2018.02.024
Received 12 April 2017; Received in revised form 1 February 2018; Accepted 16 February 2018
0010-938X/

Please cite this article as: Liu, S., Corrosion Science (2018), https://doi.org/10.1016/j.corsci.2018.02.024

Table 1
Nominal and actual composition of the tested alloys measured by ICP spectrometry analysis.

Nominal (at.%)	Actual (at.%)
Fe-19Ni-13Cr	Fe-19.4Ni-12.6Cr
Fe-19Ni-13Cr-2Al	Fe-19.3Ni-12.8Cr-2.3Al
Fe-19Ni-13Cr-6Al	Fe-18.6Ni-12.7Cr-6Al
Fe-19Ni-21Cr	Fe-19.2Ni-20.8Cr
Fe-19Ni-21Cr-2Al	Fe-18.9Ni-20.6Cr-2.2Al
Fe-19Ni-21Cr-6Al	Fe-18.6Ni-19.7Cr-6Al

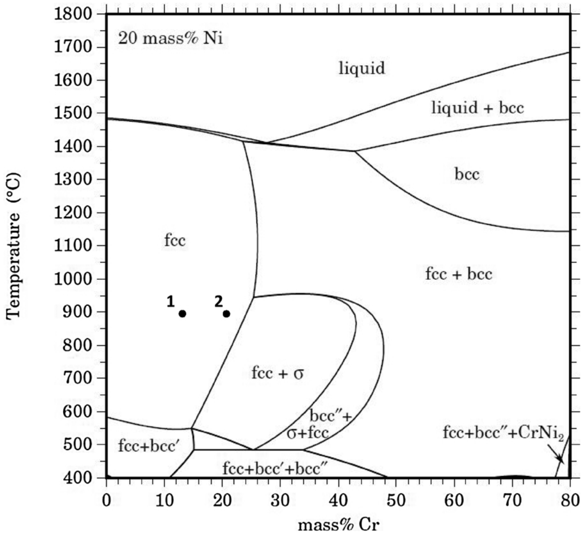

Fig. 1. Ternary phase diagram of Fe-20Ni-Cr (mass %) alloys [11] with an indication of the composition of the alloys examined in this paper (Fe-19Ni-13Cr: Point 1; Fe-19Ni-21Cr: Point 2).

Table 2
Initial compositions of the gas mixtures (I and II) and calculated values of the carbon activity and oxygen pressure after equilibration at 900 °C.

	Gas I	Gas II
CH_4 (vol.%)	25.5	10
H_2 (vol.%)	56.5	90
CO_2 (vol.%)	18	0
a_C	6.1	6
P_{O2} (atm)	1.22×10^{-22}	$\leq 10^{-30}$[a]
Impurities In Gas II		$O_2 \leq 1$ ppm $CO \leq 0.18$ ppm $CO_2 \leq 0.18$ ppm $H_2O \leq 2.9$ ppm

[a] The oxygen pressure in Gas II is calculated according to the content of the impurities.

successively finer abrasive papers down to 2000 grit and finally cleaned with water, acetone and ethanol and dried immediately before each test. Corrosion tests were carried out in a microbalance Setaram B-92 using a Pt catalyst at 900 °C in a gas mixture of (vol.%) 25.5CH_4-56.5H_2-18CO_2 providing at equilibrium a carbon activity of 6.1 and an oxygen pressure of 1.22×10^{-22} atm. The gases were premixed before entering in the reaction chamber. The duration of all tests was of 20 h. The samples were put into the furnace after the temperature reached 900 °C. Moreover, in order to explore the role of oxygen, all alloys were also exposed for 20 h to a gas mixture of (vol.%) 10CH_4-bal.H_2 which nominally contains only one oxidant carbon plus oxygen impurities, shown in Table 2. providing an oxygen pressure of about 10^{-30} atm [12], higher than the dissociation pressure of Al_2O_3, but lower than that of Cr_2O_3. This purely carburizing atmosphere provides a carbon activity $a_C = 6$, similar to that produced by the above carburizing-oxidizing atmosphere ($a_C = 6.1$).

The calculated values of a_C and P_{O2} are shown in Table 2. At high temperatures, the carbon activities and the oxygen pressures in the carburizing-oxidizing atmosphere could be calculated using the conditions of virtual equilibrium of the following reactions:

$$CH_4 = C + 2H_2 \quad (1)$$

$$2CO_2 = 2CO + O_2 \quad (2)$$

$$2CH_4 + O_2 = 2CO + 4H_2 \quad (3)$$

The corroded samples were examined by means of scanning electron microscopy (SEM) (FEI INSPECTF 50, USA, HV: 25 kV), generally using the back-scattered electron image (BEI) mode, energy dispersive X-ray microanalysis (EDX, OXFORD X-Max, UK), XRD (Panalytical X'Pert PRO, Holland, Kα-Cu radiation) and optical metallography (OM, Carl Zeiss Axio Observer. Z1m) to study the structure of the scales, to identify the nature of the phases and their distribution and for elemental analysis. The reacted samples were etched with Murakami's etchant to reveal the precipitated carbides.

3. Corrosion kinetics

The kinetic curves for the corrosion of all alloys exposed to the carburizing-oxidizing atmosphere at 900 °C are shown separately in Fig. 2a and c as linear plots and in Fig. 2b and d as parabolic plots, respectively.

The kinetic curves of Fe-19Ni-13Cr (Fig. 2a, b) obeyed a multi-step parabolic rate law. An initial stage of about 2.5 h with an instantaneous parabolic rate parameter (iprp) increasing with time was followed by two parabolic stages: the first, lasting from 2.5 to 9 h, with a parabolic rate constant k_p equal to $1.71 \times 10^{-9}\,g^2\,cm^{-4}\,s^{-1}$, and the second, lasting from 9 to 20 h, with a $k_p = 1.12 \times 10^{-9}\,g^2\,cm^{-4}\,s^{-1}$. A similar behavior was shown by Fe-19Ni-13Cr-2Al (Fig. 2a, b): an initial stage with an iprp increasing with time was followed by two parabolic periods: the first, lasting from 2.5 to 9 h, with a parabolic rate constant k_p equal to $3.2 \times 10^{-9}\,g^2\,cm^{-4}\,s^{-1}$, and the second, lasting from 9 to 20 h, with a $k_p = 1.29 \times 10^{-9}\,g^2\,cm^{-4}\,s^{-1}$. The corrosion kinetics of Fe-19Ni-13Cr-6Al (Fig. 2a, b) showed an initial period of iprp increasing with time followed by a single parabolic stage with $k_p = 1.43 \times 10^{-12}\,g^2\,cm^{-4}\,s^{-1}$.

The kinetic curves for Fe-19Ni-21Cr (Fig. 2c, d) followed a single parabolic stage with $k_p = 7.6 \times 10^{-10}\,g^2\,cm^{-4}\,s^{-1}$ after an initial period of about 6 h with an iprp increasing with time. The kinetics of Fe-19Ni-21Cr-2Al showed two parabolic stages after an initial period of about 4 h with an iprp increasing with time: the first, lasting from 4 to 9 h, with parabolic rate constant $k_p = 2.33 \times 10^{-10}\,g^2\,cm^{-4}\,s^{-1}$ and the second, lasting from 13 to 20 h, with $k_p = 1.78 \times 10^{-11}\,g^2\,cm^{-4}\,s^{-1}$. Corrosion of the Fe-19Ni-21Cr-6Al (Fig. 2c, d) showed a short initial stage of about 1 h, followed by a parabolic stage with $k_p = 2.65 \times 10^{-13}\,g^2\,cm^{-4}\,s^{-1}$. The initial and final times for each stage as well as the corresponding k_p values for all alloys are shown in Table 3.

For the alloys with 13% Cr (Fig. 2a, b) exposed to the carburizing-oxidizing atmosphere, the addition of 2% Al did not improve the corrosion resistance, but induced a slightly increase of the total mass gain. However, an increase of the aluminum content to 6% significantly improved the corrosion resistance by reducing markedly the total mass gain, but particularly by producing a large decrease of the parabolic rate constant. Conversely for the alloys with 21% Cr (Fig. 2c, d), the mass gain decreased in all cases quite effectively with an increase of the aluminum content, especially for an addition of 6% Al.

In all cases the increase of the chromium content from 13 to 21% produced a decrease of the total mass gain for a constant aluminum content, showing that the presence of chromium is beneficial for protecting the alloys from the carbon attack in this atmosphere (shown in Fig. 3).